Research Article
doi.org/10.1002/celc.202200815

Chemistry Europe
European Chemical Societies Publishing

www.chemelectrochem.org

Influence of Lithium Difluoro (Oxalato) Borate Additive on the Performance of $LiCoPO_4$—$LiFePO_4$ Solid-Solution by Carbothermal Reduction

Sreekumar Sreedeep,[a] Selvarasu Praneetha,[a] Yun-Sung Lee,*[b] and Vanchiappan Aravindan*[a]

We report the effect of lithium difluoro (oxalato) borate (LiDFOB) additive on the electrochemical performance of $LiFe_{0.5}Co_{0.5}PO_4$@C, along with the fabrication of a full-cell with $Li_4Ti_5O_{12}$ (LTO) anode. Here, we used a scalable carbothermal reduction for the synthesis of $LiCoPO_4$—$LiFePO_4$ solid-solution, $LiFe_{0.5}Co_{0.5}PO_4$@C. The electrochemical activity of $LiFe_{0.5}Co_{0.5}PO_4$@C cathode is studied by varying LiDFOB (up to 2 wt%) concentration and showed significant improvement compared to the normal electrolyte in half-cell assembly. Among the various concentrations of LiDFOB, 1.5 and 2 wt% additions are optimized owing to the higher discharge capacity of 114 and 116 mAh g^{-1} with a capacity retention of 65 and 73% after 60 cycles, respectively. The Li^+ ion diffusion coefficients are calculated from both cyclic voltammetry and impedance spectroscopy analysis and show a decrease in the value as the concentration of LiDFOB is increased from 0.5 to 2 wt%, with an order of magnitude in the range of ~10^{-14} cm^2 s^{-1}. The full-cell, $LiFe_{0.5}Co_{0.5}PO_4$@C/LTO is also fabricated and displayed a discharge capacity of 95 mAh g^{-1}. The possibility of using such full-cell assembly with various temperature conditions is studied from −10 to 25 °C.

Introduction

Energy is one of the prime concerns of the modern world, and the quest for an ideal energy storage system is still going on. The fossil fuels such as coal and petroleum have served as a major source of energy, but the overexploitation of these resources has led to their depletion.[1–3] Also, the increased usage of fossil fuels has resulted in serious environmental concerns such as the greenhouse effect and air pollution.[4–7] Therefore, the transition towards more economical, sustainable, and eco-friendly energy sources is necessary to meet the current energy demand of the modern world.[7] Energy storage systems, especially batteries, are a potential alternative to primitive fossil fuel technology. Lithium-ion batteries (LIBs) have emerged as prominent energy storage devices owing to their high energy density, lightweight, and environmental friendliness. LIB's are widely applied in various applications, prominent among which are portable electronic devices and also in zero-emission electric as well as hybrid electric vehicles (EV's and HEV's).[7,8] As there is a growing demand for LIB's improvement of various parameters, especially energy density with much more safety features is of current research interest. Thus, $LiCoO_2$ owing to the energy density of ~150 Wh kg^{-1}, has been widely used as a cathode material during the early stage of its development. But the wide range of applications of $LiCoO_2$ has been hindered due to its high cost, safety concerns, and low redox potential.[9,10] The olivine-structured $LiMPO_4$ (M: Mn, Fe, Co, and Ni) has emerged as a potential alternative for $LiCoO_2$.[3,7,11–14] The high energy density, high redox potential, and excellent thermal stability possessed by the olivine class attracted a lot of research interest. Although the commercialization of $LiFePO_4$ has been achieved, the low redox potential of the $Fe^{3+/2+}$ couple (3.4 V *vs.* Li) results in a poor energy density of ~580 Wh kg^{-1}.[15–17] These shortcomings associated with $LiFePO_4$ encouraged the research of other members of the olivine family, especially $LiCoPO_4$. The $LiCoPO_4$ owing to the excellent redox potential of the $Co^{3+/2+}$ of 4.8 V *vs.* Li, the theoretical capacity of 164 mAh g^{-1}, and energy density of ~800 Wh kg^{-1} have made it a promising candidate among the olivine class.[4,9,10,18] In addition, the high thermal stability due to the strong P—O covalent bond of the PO_4^{3-} anion has made it more attractive. However, the development of $LiCoPO_4$ is hindered due to low electronic and ionic conductivity, poor compatibility with electrolyte solution, and the fast fading of capacity. Therefore various strategies such as carbon coating,[19–23] particle size reduction,[9] and metal-doping[24–28] are employed to mitigate the issues associated with $LiCoPO_4$

Although found attractive among the different strategies, the method of metal-ion doping, as well as electrolyte optimization, are found to be more promising. Metal-ion doping, particularly Fe-doping, aims at improving the bulk Li^+ ion as well as electronic conduction in $LiCoPO_4$. In addition, the

[a] S. Sreedeep, Dr. S. Praneetha, Dr. V. Aravindan
Department of Chemistry
Indian Institute of Science Education and Research (IISER]
Tirupati 517507, India
E-mail: aravindan@iisertirupati.ac.in
Homepage: https://aravindvan2.wixsite.com/aravindlab
[b] Prof. Y.-S. Lee
School of Chemical Engineering
Chonnam National University
Gwang-ju, 61186, Republic of Korea
E-mail: leeys@chonnam.ac.kr
Homepage: http://leeys.jnu.ac.kr/eng/pro/pro.php

Supporting information for this article is available on the WWW under https://doi.org/10.1002/celc.202200815

preferential occupation of Fe in the *4c* site will suppress the Li–Co anti-site exchange, thereby overcoming the issue of low cycle stability.[25,29–31] Along with the method of Fe-doping, the optimization of electrolytes is also found to be effective in the case of $LiCoPO_4$. The preferential decomposition of the additives results in the formation of a stable solid-electrolyte interphase (SEI) which prevents the decomposition of electrolytes, hence mitigating the issue of irreversible capacity loss (ICL). Along with that, the passivating SEI layer will prevent the nucleophilic attack of F^-anions, hence protecting the degradation of the lattice.[10,32–35] Lithium difluoro (oxalate) borate (LiDFOB) is one such additive that can assist in the formation of a stable SEI layer, thereby improving the cycle stability of $LiCoPO_4$. Meng *et al.*[36,37] had shown that the use of LiDFOB had enhanced the initial discharge capacity to 138 $mAh\,g^{-1}$ with an excellent capacity retention of 69.4% after 40 cycles. In addition, the high solubility of LiDFOB in carbonate electrolytes made it more effective compared to other boron additives such as lithium bis(oxalate)borate.[5,38]

Taking into account the various challenges associated with $LiCoPO_4$, here we are attempting to improve the electrochemical performance of $LiCoPO_4$ by combining the strategy of Fe-doping along with electrolyte optimization using LiDFOB as an additive. A scalable carbothermal approach[39] has been employed for the synthesis of $LiCoPO_4$–$LiFePO_4$ solid-solution, $LiFe_{0.5}Co_{0.5}PO_4$@C. Also, to prove the fact of enhanced Li^+ ion conduction upon Fe doping, the calculation of Li^+ ion diffusion coefficient has been carried out from both Cyclic voltammetry (CV) as well as impedance studies. Along with this, the fabrication of full-cell has been carried out with $Li_4Ti_5O_{12}$ as the anode, and the temperature study has also been carried out within the range of −10 to 20 °C.

Results and discussion

The XRD analysis (Figure 1a) of solid-solution between $LiFePO_4$–$LiCoPO_4$ ($LiFe_xCo_{1-x}PO_4$@C, $0<x<0.5$) phases has been carried out to determine the structural features of the sample. Also, it can be further pointed out that no secondary phase reflections were observed, which clearly indicates the phase purity of the powders prepared, whereas all the peaks are very well matching with the diffraction patterns of $LiCoPO_4$. Along with that, the prominent reflection peaks observed at 2θ values of 35.69, 29.95, and 25.72 corresponds to the crystal planes of (311), (211), and (201), further suggesting the formation of an

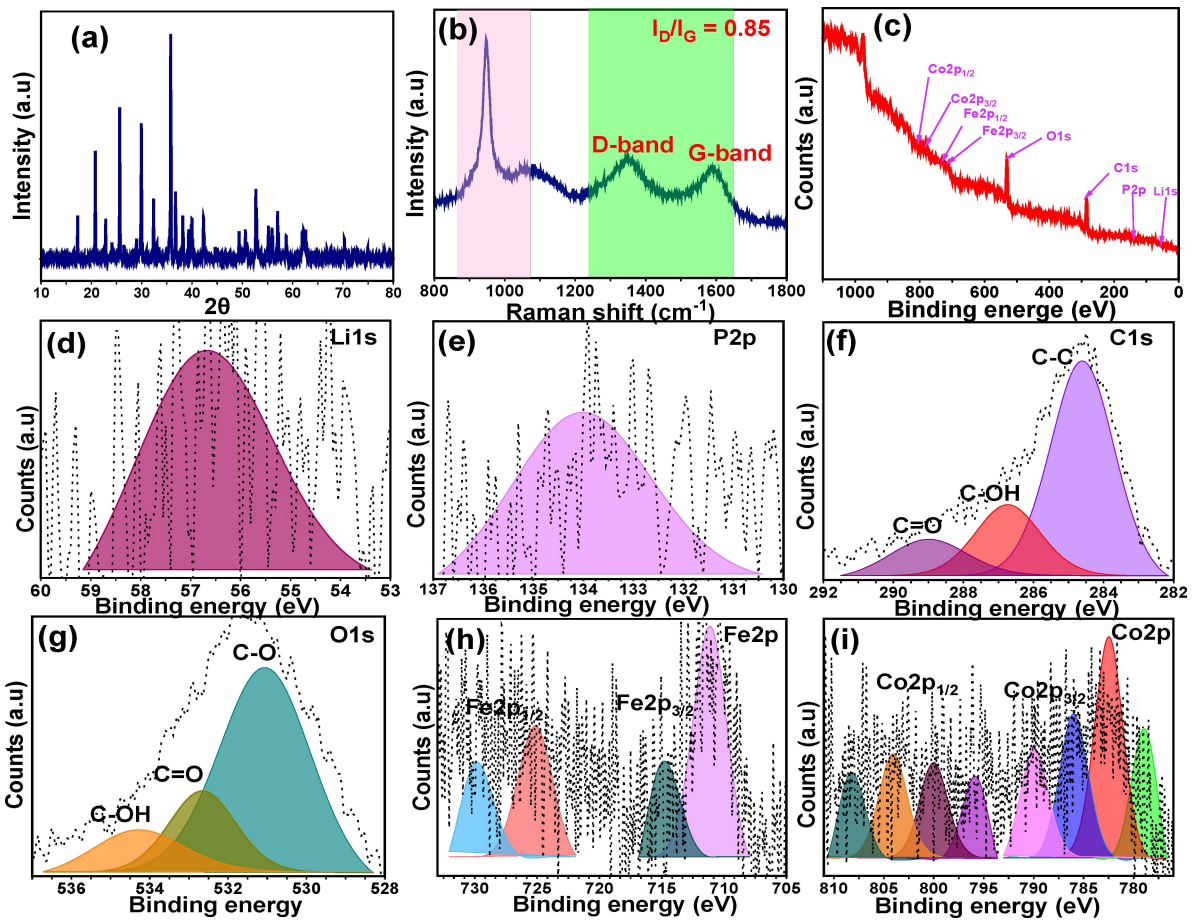

Figure 1. (a) XRD spectra of $LiFe_{0.5}Co_{0.5}PO_4$@C (b) Raman spectra of $LiFe_{0.5}Co_{0.5}PO_4$@C showing the peaks corresponding to PO_4^{3-} anion (highlighted in pink), D and G-band (highlighted in green), (c) XPS spectra of the as-synthesized $LiFe_{0.5}Co_{0.5}PO_4$@C, and (d-i) deconvoluted XPS spectra of Li 1s, P 2p, C 1s, O 1s, Fe 2p, and Co 2p.

orthorhombic lattice with a *Pnma* space group (ICDD No: 89–6192).[4,9] Also, the unit cell parameters have been calculated using Rietveld refinement as $a = 10.27$ Å, $b = 5.94$ Å, and $c = 4.74$ Å along with the cell volume of $V = 289.5$ Å^3.

The surface elemental composition of the sample has been examined using XPS. The XPS survey spectra have indicated the presence of elements such as Li, Co, Fe, C, O, and P (Figure 1c) Now, deconvolution of the Li 1s, Co 2p, Fe 2p, C 1s, O 1s, and P 2p has been done to determine the chemical/oxidation state of the elements[27,40](Figure 1d–i). The C 1s core level can be decomposed into peaks at 284.6, 286.74, and 289.01 eV, which corresponds to the C–C, C–OH, and C=O functional groups, respectively. The deconvolution of O 1s core level produces peaks at 531.04, 532.65, and 534.04 eV corresponding to C–O, C=O, and C–OH coordination, respectively. The spectra of Fe2p exhibits two pair of peaks belonging to the $FeP_{1/2}$ and Fe $P_{3/2}$ at 714 and 729 eV, whereas the Co 2p shows peaks at 789 and 800 eV corresponding to the Co $P_{1/2}$ and Co $P_{3/2}$ states. Hence, this confirms the presence of Fe^{2+} and Co^{2+} in the as-synthesized compound. However, the Li 1s and P 2p exhibit single broad peaks positioned at 56 and 134 eV, which reveals the presence of +1 and +5 oxidation states in Li as well as P, respectively. The Raman spectral analysis (Figure 1b) of $LiFe_{0.5}Co_{0.5}PO_4$@C exhibits the characteristic peaks at ~1352 and 1592 cm^{-1} corresponding to the D and G-band, indicating the disordered and graphitized state of carbon, respectively. Also, the degree of disorderliness evaluated from the ratio of the intensity of the D-band to the G-band (I_D/I_G) comes out to be 0.85, which suggests the presence of the crystalline nature of carbonaceous material.[27] The carbon content in the sample has been further quantified using the TGA (Figure S1) analysis as ~ 4.9 wt%. In addition, the more prominent peak at 950 cm^{-1} indicates the symmetric P–O bond in PO_4^{3-} anion, whereas the less intense peak at 596 cm^{-1} indicates the Fe dopant in the sample.[41,42]

Imaging techniques such as FE-SEM and TEM have been carried out to reveal the morphology and structural features of $LiFe_{0.5}Co_{0.5}PO_4$@C. The SEM image (Figure 2a–c) depicts a non-uniform size distribution owing to the agglomeration of particles, with the particulate size of ~418 nm. The FE-SEM image also reveals that a homogeneous carbon layer has been formed on the surface of the sample, which is further revealed from the TEM analysis (Figure 2d–f). Also, the lattice fringe width or *d* spacing (Figure 2f) has been determined from the TEM image as 0.349 nm, which corresponds to the (111) crystal plane of $LiCoPO_4$. The SAED (Figure 2e) pattern also reveals the formation of a highly crystalline compound. In addition, the energy dispersion X-ray spectroscopy (EDS) (Figure 2g–k) analysis depicts the uniform distribution of elements such as Li, Co, Fe, P, O, and C in the sample. Hence, all these techniques,

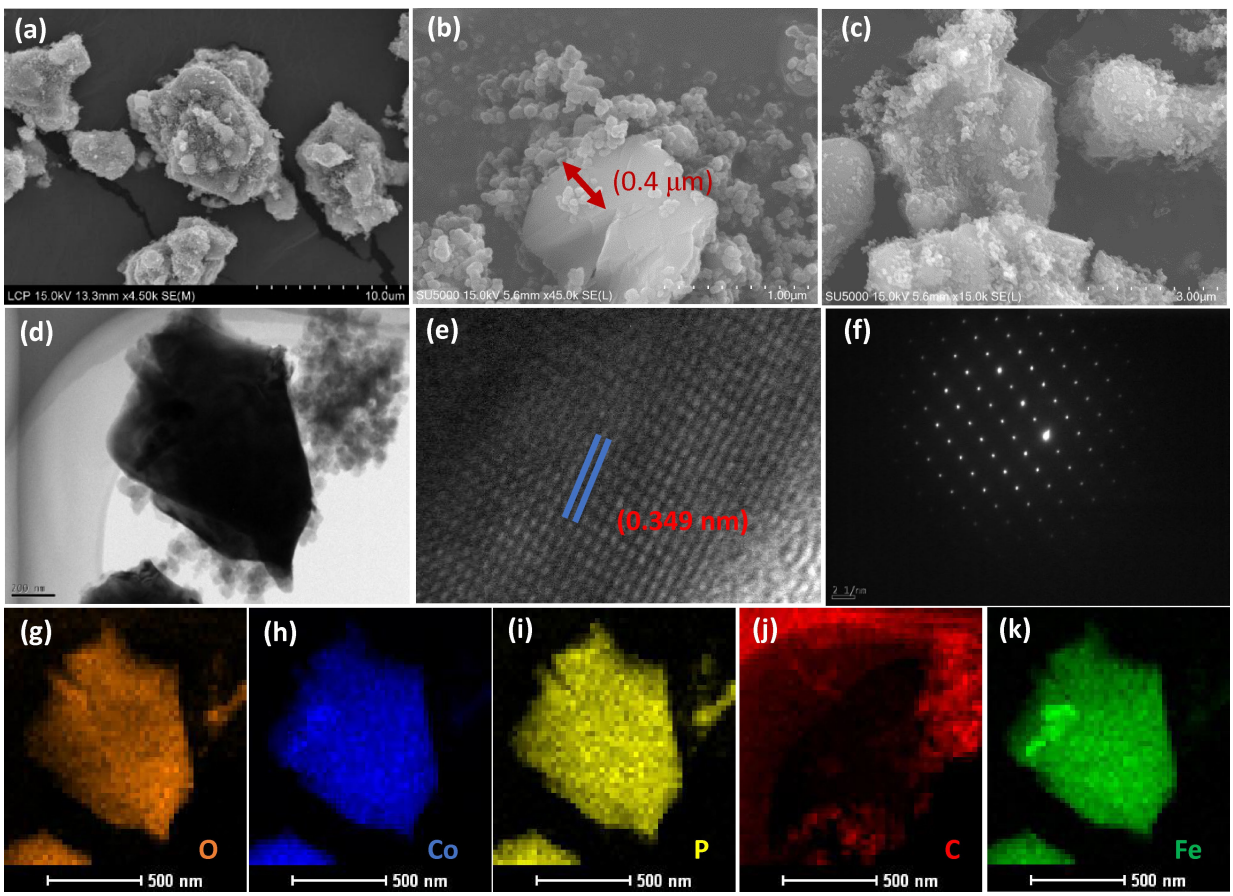

Figure 2. (a-c) FE-SEM images of $LiFe_{0.5}Co_{0.5}PO_4$@C, (d and f) TEM images of $LiFe_{0.5}Co_{0.5}PO_4$@C, (e) SAED pattern of $LiFe_{0.5}Co_{0.5}PO_4$@C, (g-k) EDS mapping of $LiFe_{0.5}Co_{0.5}PO_4$@C showing the elemental distribution of O, Co, P, C, and Fe in the sample.

including XRD, XPS, SEM, TEM, and EDS studies, confirm the formation of $LiFe_{0.5}Co_{0.5}PO_4$@C.

Half-cell performance

The electrochemical performance of the $LiFe_{0.5}Co_{0.5}PO_4$@C cathode has been carried out in half-cell assembly at a current density of 20 mA g^{-1} within a potential window of 2.7-5.2 V *vs.* Li by varying the LiDFOB concentrations from 0–2 wt%. The cycling profile data (Figure 3a-b) exhibits an enhancement in the discharge capacity as well as cycle stability for the $LiFe_{0.5}Co_{0.5}PO_4$@C cycled in LiDFOB-containing electrolyte compared to that of normal electrolyte. This improvement in the electrochemical performance can be attributed to the formation of a stable SEI layer by the decomposition of LiDFOB prior to that of electrolyte, thereby mitigating the issue of huge irreversibility as well as electrolyte decomposition at higher potential. However, there are many mechanisms for explaining the formation of a stable SEI layer by LiDFOB, prevalent among which is that at the high voltage, the decomposition of LiDFOB results in the formation of reactive oxygen radicals, which reacts with the carbonate components (EC, DMC) to form carbonate containing polymeric species. Since, the HF is produced by $LiPF_6$ via hydrolysis, even with the trace amount of moisture content that consumes Li^+ from the cathode to form a resistive LiF component of the SEI layer (Eqn. 1 & 2). The use of LiDFOB certainly prevents the direct contact of the HF with the cathode, hence improving the electrochemical performance.[43] Among the various LiDFOB concentrations, the 1.5 and 2 wt% of LiDFOB exhibit higher discharge capacity of ~114 and 116 mAh g^{-1}, respectively, with a capacity retention of ~65 and 73% after 60 cycles. However, the $LiFe_{0.5}Co_{0.5}PO_4$@C, in the absence of LiDFOB, exhibits an initial discharge capacity of ~96 mAh g^{-1} with a capacity retention of 60%, which is much lower compared to that of 2 and 3 wt%.

$$LiPF_6\ (sol.) + H_2O \rightarrow POF_3\ (sol.) + LiF\ (s) + HF\ (sol.) \quad (1)$$

$$PF_5\ (sol.) + H_2O \rightarrow POF_3\ (sol.) + 2HF\ (sol.) \quad (2)$$

Apart from this, cyclic voltammetry (CV) (Figure 4a and S2) has been performed at a scan rate of 0.1 mV s^{-1} to determine the redox reactions accompanying the charge-discharge process. The CV of $LiFe_{0.5}Co_{0.5}PO_4$@C exhibits two pairs of oxidation peaks at 4.9 and 3.6 V (*vs.* Li) and two pairs of reduction peaks

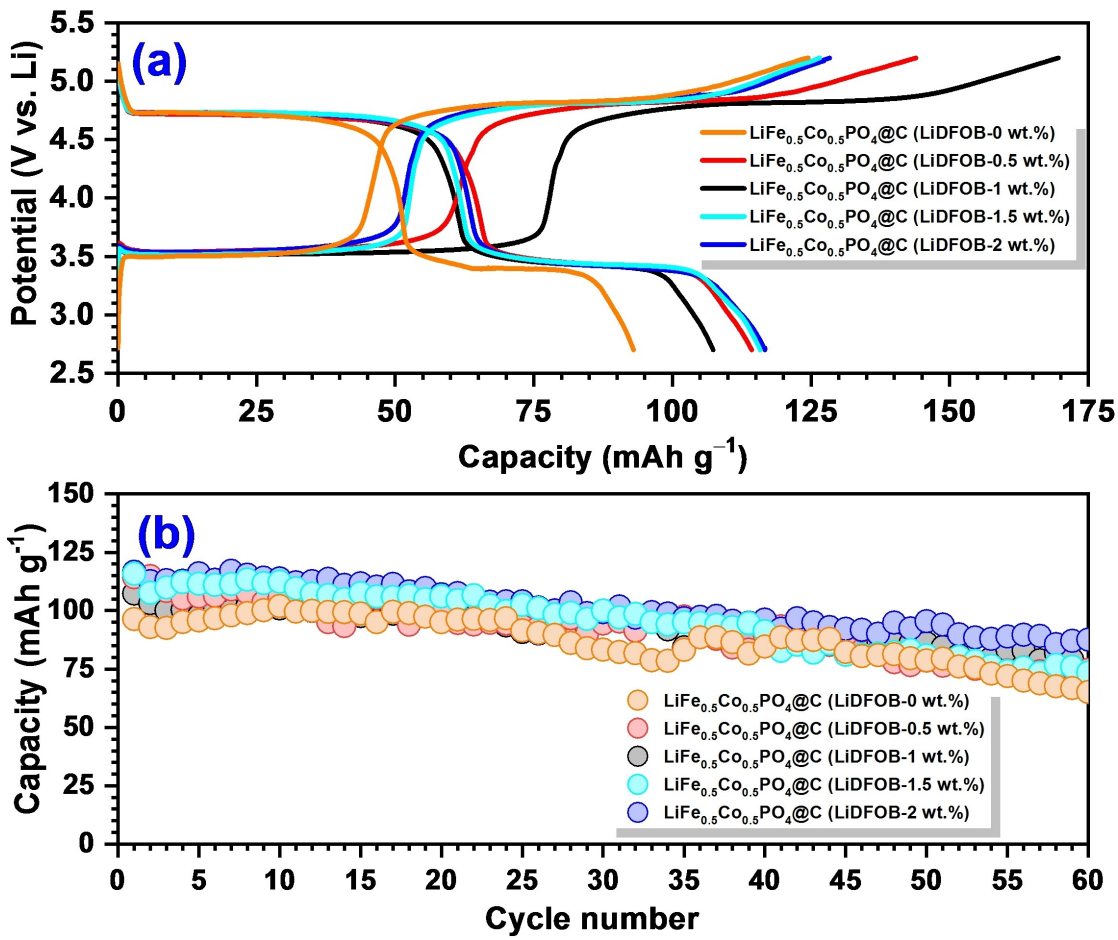

Figure 3. (a) The charge-discharge curve of $LiFe_{0.5}Co_{0.5}PO_4$@C in half-cell assembly with different LiDFOB concentrations and (b) Capacity *vs.* cycle number plots at a current density of 20 mA g^{-1} within a potential window of 2.7-5.2 V *vs.* Li.

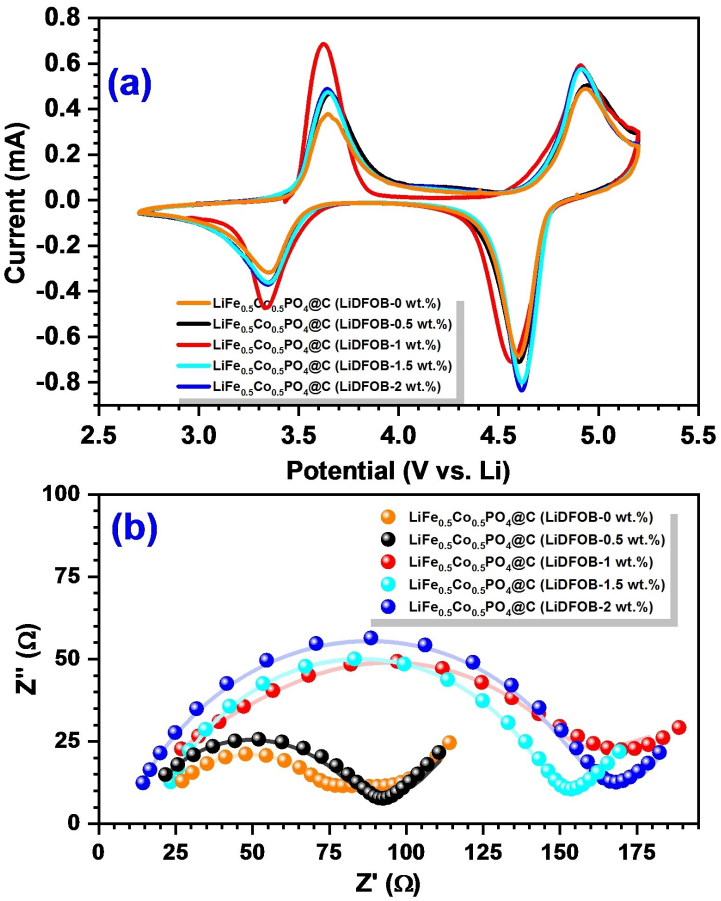

Figure 4. (a) Cyclic voltammetry traces of $LiFe_{0.5}Co_{0.5}PO_4$@C with different LiDFOB concentrations at a scan rate of 0.1 mV s^{-1} and (b) corresponding impedance curves.

positioned at 3.4 and 4.6 V (*vs.* Li) corresponding to the Co^{3+}/Co^{2+} and Fe^{3+}/Fe^{2+} redox couples and is consistent with the two plateaus observed in the galvanostatic charge-discharge of $LiFe_{0.5}Co_{0.5}PO_4$@C. However, an increase in polarization has been observed as the concentration of LiDFOB is increased from 0.5-2 wt% as the cycling progresses. However, it can be observed from the Nyquist plot ((Figure 4b) that as the concentration of LiDFOB is increased from 0.5 to 2 wt%, an increase in the charge-transfer resistance (R_{ct}) is observed owing to the formation of a thicker SEI layer which provides resistance to the mobility of the Li^+ ions. But a low value of R_{ct} in the case of additive-free electrolytes illustrates the absence of a robust SEI layer, thereby improving the mobility of Li^+ ions.

The rate performance study (Figure 5a–d) further illustrates the better capacity retention of both 1.5 and 2 wt% concentrations of LiDFOB even at a higher current density of 100 mA g^{-1}. Hence, it can be concluded that the concentration of LiDFOB within the range of 1.5–2 wt% is optimum for the better electrochemical performance of $LiFe_{0.5}Co_{0.5}PO_4$@C. The stability of the SEI layer has been analyzed using the *in-situ* impedance study (Figure 6a–f), which exhibits no increase in the R_{ct} value as the cycling progresses from the 1st to the 10th cycle, thus showing the stability and robust nature of the SEI layer. But as the cycling progresses towards the 50th cycle, an increase in the R_{ct} value is observed, which can be attributed to the decrease in the stability of the SEI layer, thereby increasing the irreversibility.

The apparent Li^+ ion diffusion coefficient of $LiFe_{0.5}Co_{0.5}PO_4$@C (LiDFOB: 0–2 wt%) has been determined from the Electrochemical impedance spectroscopy (EIS) (Figure S3) and CV (Figure S4). In the EIS, the diffusion coefficient is evaluated from the low-frequency Warburg region of the curve.[44,45] Now, the diffusion co-efficient $D_{Li}{}^+$ is determined using ern. (3),

$$D_{Li+} = R^2\,T^2/2\,A^2\,n^4\,F^4\,C^2\,\sigma_w{}^2 \quad (3)$$

Where R is the universal gas constant, T is the temperature, A is the cross-section area of the electrode, n is the number of Li^+ ions involved in charge-discharge, F is the Faraday constant, C is the concentration, and σ_w is the slope obtained from the plot of real impedance and the reciprocal square root of the angular frequency at low-frequency Warburg region. Now, the calculated value of $D_{Li}{}^+$ (Table T1) from the EIS falls in the order of 10^{-14} $cm^2\,s^{-1}$. In addition, it has been observed that the diffusion coefficient decreases from 3.94×10^{-14} to 1.74×10^{-14} $cm^2\,s^{-1}$ as the concentration of LiDFOB is increased from 0 to 2 wt%. Also, the $D_{Li}{}^+$ of $LiCoPO_4$ is close to 1.47×10^{-14}, which

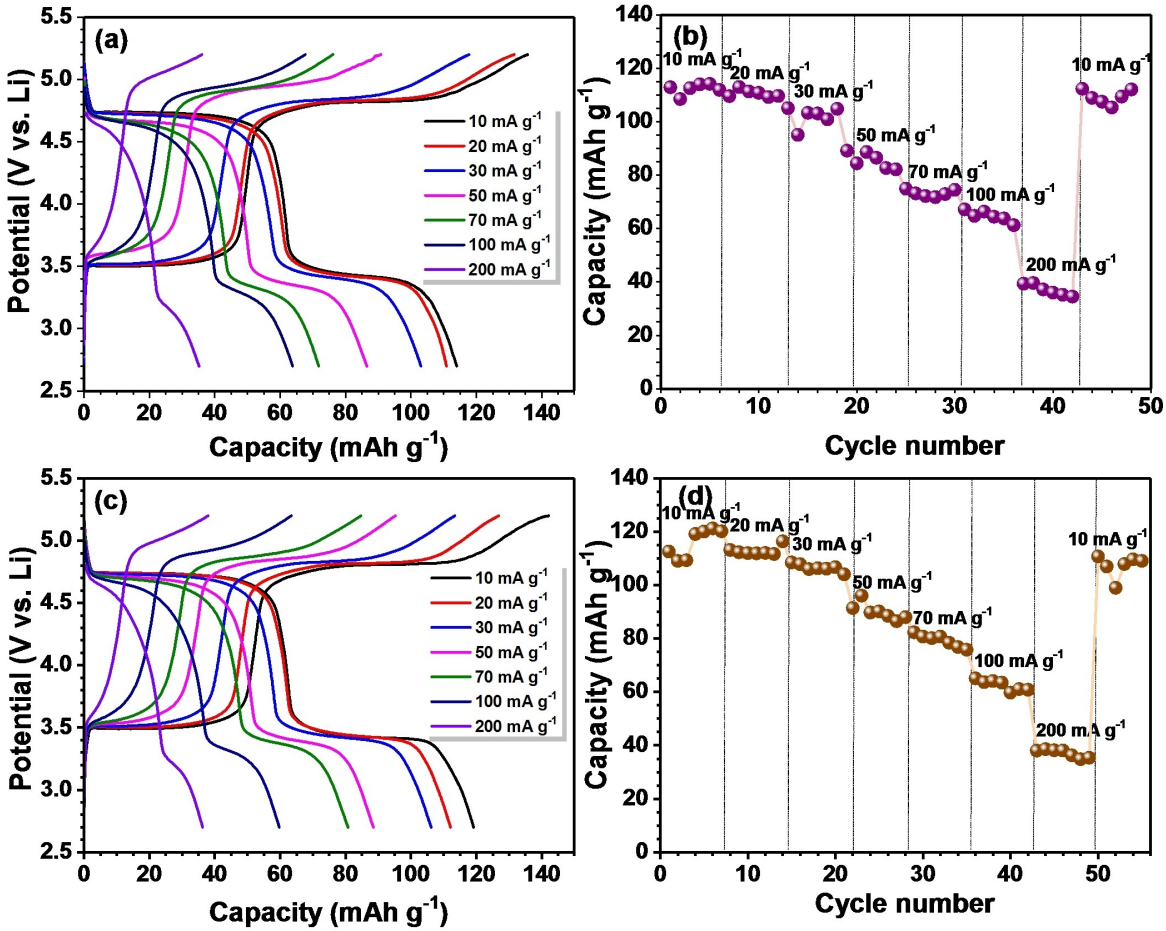

Figure 5. Rate performance study of (a-b) $LiFe_{0.5}Co_{0.5}PO_4$@C (LiDFOB: 1.5 wt%), and (c-d) $LiFe_{0.5}Co_{0.5}PO_4$@C (LiDFOB: 2 wt%) at current densities of 10, 20, 30, 50, 70, 100, and 200 mA g^{-1}.

is much lower compared to that of $LiFe_{0.5}Co_{0.5}PO_4$@C (LiDFOB: 0–2 wt%).

Parallelly, the apparent Li^+ ion diffusion coefficient for $LiFe_{0.5}Co_{0.5}PO_4$@C (LiDFOB: 0–2 wt%) has also been determined from the CV by varying the scan rate from 0.1 to 1 mV s^{-1}. The peak current observed for both cathodic as well as anodic has been evaluated, and a graph is plotted with the peak current against the square root of the scan rate(Figure S4). Now, the diffusion co-efficient is evaluated using the Randles-Sevcik equation (eqn. 4).[14,24,27,30,39,45]

$$I_p = 2.69 \times 10^5\ n^{3/2}\ C_0\ A\ D^{1/2}\ v^{1/2} \quad (4)$$

Where I_p is the peak current, n is the number of Li^+ ions involved, C_o is the concentration of Li^+ ions, A is the cross-sectional area of the electrode, D is the diffusion coefficient, and v is the scan rate. Now, the apparent diffusion coefficient is calculated from the slope, $I_p/v^{1/2}$, of peak current *vs.* square root of the scan rate plot. From Table T2, it can be observed that the magnitude of the diffusion coefficient for LiDFOB free $LiFe_{0.5}Co_{0.5}PO_4$@C cathode is in the order of ~10^{-13} $cm^2 s^{-1}$ and is much higher compared to the diffusion coefficient of $LiFe_{0.5}Co_{0.5}PO_4$@C (LiDFOB: 0.5-2 wt%) which falls in the order of 10^{-14} $cm^2 s^{-1}$. However, the calculated value of the diffusion coefficient of $LiCoPO_4$ is of the order of 10^{-15} $cm^2 s^{-1}$, which is lower compared to that of $LiFe_{0.5}Co_{0.5}PO_4$@C (LiDFOB: 0.5-2 wt %). Also, the diffusion coefficient obtained from both CV as well as EIS shows a similar trend, with a decrease in the magnitude of the diffusion coefficient as the concentration of LiDFOB is increased from 0–2 wt%. This overall trend in diffusion coefficient for both CV as well as EIS is observed since a thicker SEI layer has been formed as the concentration of LiDFOB is increased from 0–2 wt%, thereby providing a resistance to the mobility of Li^+ ions.

Full-cell performance

Based on the preliminary half-cell studies, the $LiFe_{0.5}Co_{0.5}PO_4$@C (LiDFOB: 2 wt%) has been carried out for further full-cell studies against LTO as the anode. The mass of the cathode has been adjusted w.r.t the mass of the anode using the equation (eqn. 5)

$$m_1\ c_1 = m_2\ c_2 \quad (5)$$

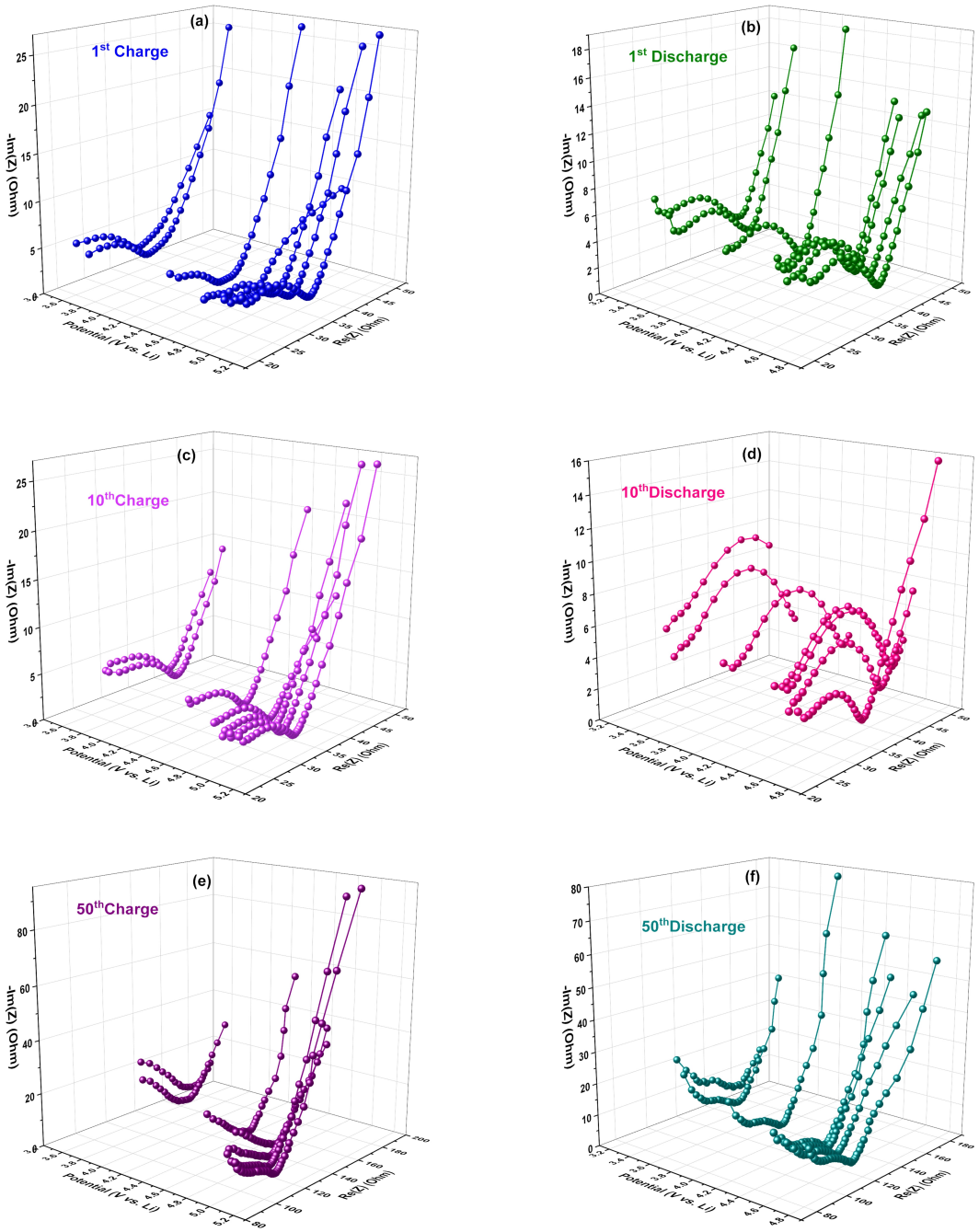

Figure 6. Plot showing the *in-situ* impedance study of $LiFe_{0.5}Co_{0.5}PO_4$@C (LiDFOB: 2 wt%) at (a–b) 1st cycle (c–d) 10th cycle, and (e–f) 50th cycle

where m_1 and m_2 are the masses of cathode and anode active materials, respectively, c_1 and c_2 are their respective capacities in $mAh\,g^{-1}$. Now, for the mitigation of irreversibility, both $LiFe_{0.5}Co_{0.5}PO_4$@C and LTO are subjected to pre-treatment for three cycles before cell assembly. The cycling profile (Figure 7a-b) of $LiFe_{0.5}Co_{0.5}PO_4$@C (LiDFOB-2 wt%)-LTO full-cell exhibits a discharge capacity of 94 $mAh\,g^{-1}$ with a capacity retention of 92% after 15 cycles. To further investigate this superior electrochemical performance, the temperature study of the same has been performed in the temperature range of −10 to 20 °C (Figure 8a-b).The $LiFe_{0.5}Co_{0.5}PO_4$@C(LiDFOB-2 wt%)-LTO full-cell exhibits poor electrochemical performance at low temperatures in the range of −10 to 0 °C owing to the decrease in Li^+ ion mobility due to freezing up of electrolyte solution.[27] On the other hand, as the temperature is increased to a moderate value of 10 and 20 °C, the full cell exhibits a discharge capacity of 85 and 55 $mAh\,g^{-1}$ with a capacity retention of 73 and 82% after 50 cycles. Further studies are in progress to improve the electrochemical activity of the solid solution by fine-tuning the additive concentration.

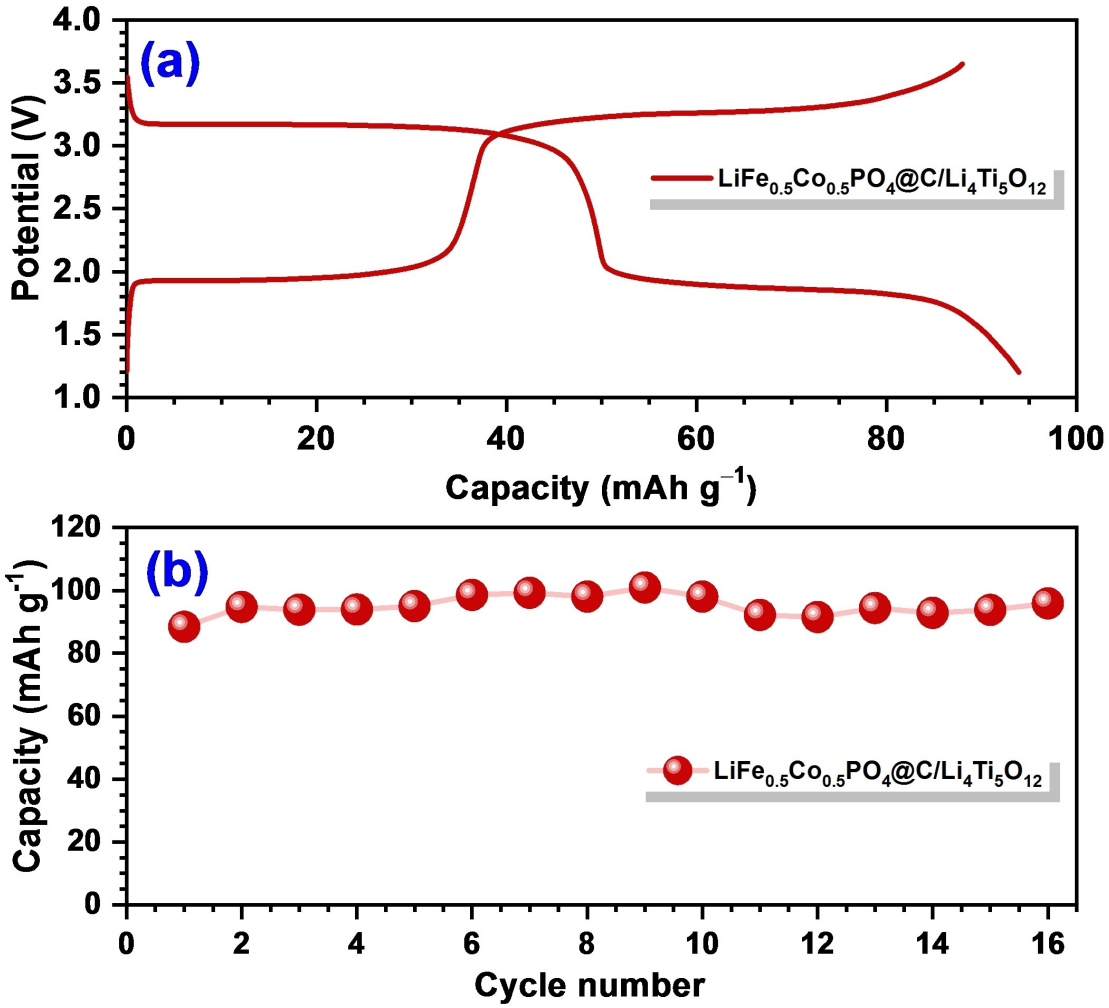

Figure 7. (a) Charge-discharge curve of $LiFe_{0.5}Co_{0.5}PO_4$@C (LiDFOB: 2 wt%)/LTO cell at a current density of 20 mA g^{-1} within a potential window of 1.2–3.6 V, and (b) discharge capacity *vs.* cycle number.

Conclusion

Here, we successfully demonstrated the effect of LiDFOB as an electrolyte additive on the electrochemical performance of carbothermal synthesized $LiFe_{0.5}Co_{0.5}PO_4$@C (LiDFOB: 0–2 wt%). The Galvanostatic charge-discharge exhibit better electrochemical performance in the case of $LiFe_{0.5}Co_{0.5}PO_4$@C (LiDFOB: 0.5–2 wt%) compared to that of a normal electrolyte. In addition, among the various LiDFOB concentrations, 1.5 and 2 wt% is found appealing owing to the high capacity retention of 65, and 73% has been optimized to show better electrochemical performance. The a.c. impedance study exhibits an increasing trend for R_{ct} as the concentration of LiDFOB is increased from 0.5 to 2 wt%, whereas a low value of R_{ct} is observed in the absence of LiDFOB. The *in-situ* impedance study further shows that as the cycling progresses towards the 60th cycle, an increase in the value of R_{ct} is observed compared to that of the 10th cycle. Li-ion diffusion coefficient is calculated from both CV as well as EIS, both of which had shown a decrease in the value of the diffusion coefficient with an increase in the concentration of LiDFOB from 0 to 2 wt%. Now, fabrication of full-cell has been done with $LiFe_{0.5}Co_{0.5}PO_4$@C (LiDFOB: 2 wt%) against LTO as the anode. Also, the cycling profile of the full-cell exhibited better electrochemical performance at a moderate temperature of 10 and 20 °C. Hence, all these results prove the superior electrochemical performance of $LiFe_{0.5}Co_{0.5}PO_4$@C in the presence of LiDFOB. However, the research on electrolyte additives has to be extended further to various phosphorus, sulfur, and carbonate-based additives to improve the electrochemical activity by stabilizing the interface. Also, further research has to be done by coupling $LiFe_{0.5}Co_{0.5}PO_4$@C with other conversion and alloying type anodes.

Experimental section

Synthesis

The solid solution, $LiFe_{0.5}Co_{0.5}PO_4$@C, has been synthesized using a reported procedure.[39] In a typical carbothermal synthesis approach, a stoichiometric amount of Li_2CO_3 (Sigma-Aldrich, ≥99%), $(NH_4)_2HPO_4$ (Sigma-Aldrich, ≥98%), Co_3O_4 (Sigma-Aldrich), $Fe(CH_3COO)_2$ (Sigma-Aldrich, ≥99.99%) has been taken. To the

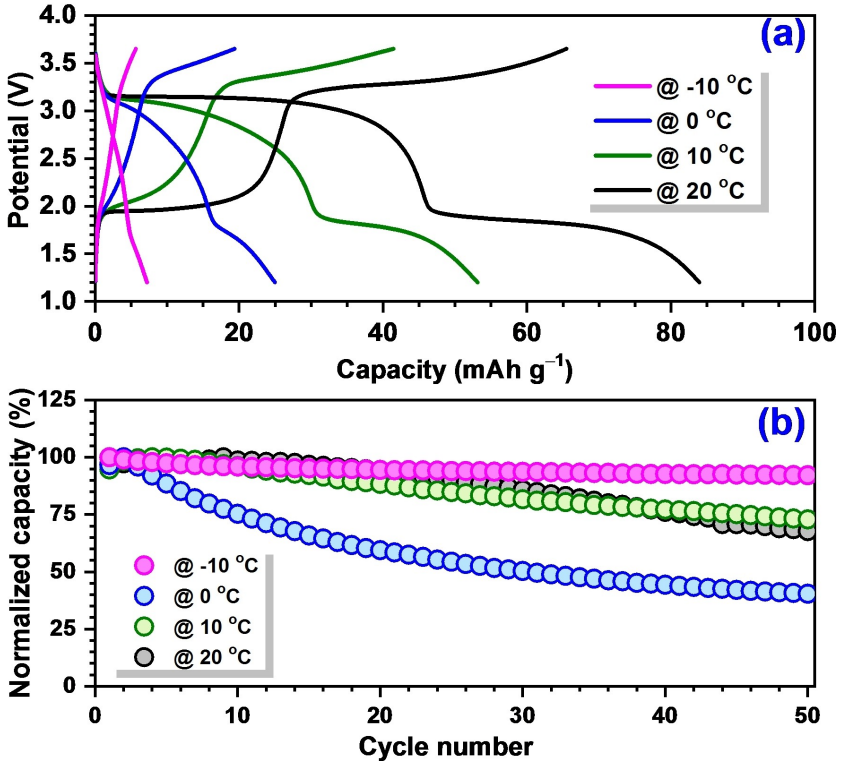

Figure 8. (a) The charge-discharge curve of $LiFe_{0.5}Co_{0.5}PO_4$@C (LiDFOB: 2 wt%)/LTO cell at a current density of 20 mA g^{-1} within a potential window of 1.2–3.6 V, and (b) discharge capacity *vs.* cycle number at temperatures ranging from −10 to 20 °C.

above precursors, conductive carbon (Super-P) (additional 5 wt%), which acts as a reducing agent, was added and grounded well. Now, the obtained mixture was subjected to ball-milling with a sample-to-ball ratio of 1:5 for a duration of 3H in a planetary ball-miller under the Argon atmosphere. The ball-milled sample was then subjected to pyrolysis to a temperature of 800 °C at a ramp rate of 2 °C min^{-1} for a duration of 2 hours under an Argon atmosphere. Now, the above-obtained mixture was grounded properly to a fine powder using a mortar and pestle.

Electrolyte preparation

The preparation of electrolytes was carried out inside a glove box with an oxygen level (< 0.1 ppm) by mixing 2500 µl of 1 M $LiPF_6$ in Ethylene Carbonate (EC) and Dimethyl carbonate (DMC) (1:1 weight ratio, LIPASTE, Tomiyama) along with 0–2 wt% of Lithium difluoro(oxalate) borate (LiDFOB) as the electrolyte additive. None of the salt or solvent was subjected to any sort of pre-treatment or purification before its usage.

Electrochemical characterization

The fabrication of full-cell and half-cell was carried out in an Argon-filled glove box (MBraun, Germany) with an oxygen and moisture level of < 0.1 ppm. For the preparation of the composite electrode 10 mg of $LiFe_{0.5}Co_{0.5}PO_4$@C, 2 mg conductive carbon (Super-P), and 2 mg of binder (TAB-2, Teflonized acetylene black) were mixed using ethanol as a medium to obtain a free-standing film. Now, the electrodes were kept overnight in a vacuum oven at a temperature of 75 °C to remove the traces of solvent, if any. The electrodes were taken inside the glove box, and cells were made inside the CR2016 coin cell using the glass microfibre separator (Whatman, 1825-047, GF/F) and Lithium metal counter electrode. Now for the fabrication of the full cell, the $Li_4Ti_5O_{12}$ (LTO) was taken on the anodic side. The LTO electrodes are made after mass-balancing by mixing 6.5 mg of active material, 1.3 mg of conductive carbon (super-P), and 1.3 mg of TAB-2 into a free-standing film. Before the fabrication of full-cell, both the LTO and $LiFe_{0.5}Co_{0.5}PO_4$@C half-cells are subjected to three cycles of charge-discharge, and both the cells are de-crimped for the removal of both electrode. Now, the full cells were fabricated with a glass microfiber separator in the CR2016 coin cell in an argon-filled glovebox. And the cell was kept for various electrochemical studies in a battery tester (Biological, France), including charge-discharge at a current density of 20 mA g^{-1}.

Material characterization

The X-ray diffraction studies (XRD, XRD, Rigaku, Smart lab 9 kW) were employed for the structural analysis of $LiFe_{0.5}Co_{0.5}PO_4$@C at a scan rate of 0.5° min^{-1} in a monochromatic Cu Kα radiation. Further, Raman spectral analysis (LabRam HR800 UV Raman microscope, Horiba Jobin- Yvon, France) was carried out to determine the material composition of the sample. The X-ray photoelectron spectroscopy (XPS, with a multilab instrument with a monochromatic Al Kα radiation hν = 1486.6 eV) was done for the surface analysis of the sample. Now, for the determination of internal and morphological characteristics of the sample, a High-resolution transmission electron microscopy (HR-TEM, TECNAI, Philips, the Netherlands, 200 keV) and field emission scanning electron microscopy (FE-SEM, S-4700, Hitachi, Japan) studies were also carried out. In addition, the Thermogravimetric analysis (TGA, Shimadzu, Japan) was also performed to determine the residual carbon content in the sample.

Acknowledgments

SS acknowledges the Council of Scientific and Industrial Research (CSIR), Govt. of India, for the Fellowship. YSL acknowledges the financial support from the National Research Foundation of Korea (NRF) grant funded by the Korean government (Ministry of Science, ICT & Future Planning) (No. 2019R1 A2C1007620). VA acknowledges financial support from the Science and Engineering Research Board, a statutory body of the Department of Science & Technology, Govt. of India, through the Ramanujan Fellowship (SB/S2/RJN-088/2016) and Swarnajayanti Fellowship (SB/SJF/2020-21/12).

Conflict of Interest

The authors declare no conflict of interest.

Data Availability Statement

The data that support the findings of this study are available from the corresponding author upon reasonable request.

Keywords: cathode · high voltage · LiDFOB · Li-ion battery · olivine · solid-solution

[1] J. B. Goodenough, Y. Kim, *Chem. Mater.* **2010**, *22*, 587–603.
[2] L. Wu, S. Shi, X. Zhang, J. Liu, D. Chen, H. Ding, S. Zhong, *Mater. Lett.* **2015**, *152*, 228–231.
[3] N. Nitta, F. Wu, J. T. Lee, G. Yushin, *Mater. Today* **2015**, *18*, 252–264.
[4] J. Ludwig, T. Nilges, *J. Power Sources* **2018**, *382*, 101–115.
[5] V. Aravindan, J. Gnanaraj, S. Madhavi, H. K. Liu, *Chem. Eur. J.* **2011**, *17*, 14326–14346.
[6] B. Diouf, R. Pode, *Renewable Energy* **2015**, *76*, 375–380.
[7] V. Etacheri, R. Marom, R. Elazari, G. Salitra, D. Aurbach, *Energy Environ. Sci.* **2011**, *4*, 3243–3262.
[8] D. Deng, *Energy Sci. Eng.* **2015**, *3*, 385–418.
[9] M. Zhang, N. Garcia-Araez, A. L. Hector, *J. Mater. Chem. A* **2018**, *6*, 14483–14517.
[10] S. Sreedeep, S. Natarajan, V. Aravindan, *Curr. Opin. Electrochem.* **2022**, *31*, 100868.
[11] N. Tolganbek, Y. Yerkinbekova, S. Kalybekkyzy, Z. Bakenov, A. Mentbayeva, *J. Alloys Compd.* **2021**, *882*, 160774.
[12] P. R. Kumar, V. Madhusudhan Rao, B. Nageswararao, M. Venkateswarlu, N. Satyanarayana, *J. Solid State Electrochem.* **2016**, *20*, 1855–1863.
[13] V. Aravindan, J. Gnanaraj, Y. S. Lee, S. Madhavi, *J. Mater. Chem. A* **2013**, *1*, 3518–3539.
[14] W. F. Howard, R. M. Spotnitz, *J. Power Sources* **2007**, *165*, 887–891.
[15] Z. Yang, Y. Dai, S. Wang, J. Yu, *J. Mater. Chem. A* **2016**, *4*, 18210–18222.
[16] F. C. Strobridge, H. Liu, M. Leskes, O. J. Borkiewicz, K. M. Wiaderek, P. J. Chupas, K. W. Chapman, C. P. Grey, *Chem. Mater.* **2016**, *28*, 3676–3690.
[17] F. Yu, L. Zhang, Y. Li, Y. An, M. Zhu, B. Dai, *RSC Adv.* **2014**, *4*, 54576–54602.
[18] N. N. Bramnik, K. G. Bramnik, T. Buhrmester, C. Baehtz, H. Ehrenberg, H. Fuess, *J. Solid State Electrochem.* **2004**, *8*, 558–564.
[19] S. Sreedeep, V. Aravindan, *Mater. Lett.* **2021**, *291*, 1–4.
[20] J. Wolfenstine, J. Read, J. L. Allen, *J. Power Sources* **2007**, *163*, 1070–1073.
[21] A. Örnek, A. Yeşildağ, M. Can, S. Aktürk, *Mater. Res. Bull.* **2016**, *83*, 1–11.
[22] N. Laszczynski, A. Birrozzi, K. Maranski, M. Copley, M. E. Schuster, S. Passerini, *J. Mater. Chem. A* **2016**, *4*, 17121–17128.
[23] J. Liu, T. E. Conry, X. Song, L. Yang, M. M. Doeff, T. J. Richardson, *J. Mater. Chem.* **2011**, *21*, 9984–9987.
[24] S. Brutti, J. Manzi, D. Meggiolaro, F. M. Vitucci, F. Trequattrini, A. Paolone, O. Palumbo, *J. Mater. Chem. A* **2017**, *5*, 14020–14030.
[25] J. Wolfenstine, *J. Power Sources* **2006**, *158*, 1431–1435.
[26] F. Wang, J. Yang, Y. NuLi, J. Wang, *J. Power Sources* **2010**, *195*, 6884–6887.
[27] S. Sreedeep, S. Natarajan, Y.-S. Lee, V. Aravindan, *Electrochim. Acta* **2022**, *419*, 140367.
[28] D. Di Lecce, J. Manzi, F. M. Vitucci, A. De Bonis, S. Panero, S. Brutti, *Electrochim. Acta* **2015**, *185*, 17–27.
[29] D. Han, Y. Kang, R. Yin, M. Song, H. Kwon, *Electrochem. Commun.* **2009**, *11*, 137–140.
[30] J. L. Allen, T. Thompson, J. Sakamoto, C. R. Becker, T. R. Jow, J. Wolfenstine, *J. Power Sources* **2014**, *254*, 204–208.
[31] J. L. Allen, T. R. Jow, J. Wolfenstine, *J. Power Sources* **2011**, *196*, 8656–8661.
[32] Y. Maeyoshi, S. Miyamoto, Y. Noda, H. Munakata, K. Kanamura, *J. Power Sources* **2017**, *337*, 92–99.
[33] A. M. Haregewoin, A. S. Wotango, B. J. Hwang, *Energy Environ. Sci.* **2016**, *9*, 1955–1988.
[34] L. Yang, T. Markmaitree, B. L. Lucht, *J. Power Sources* **2011**, *196*, 2251–2254.
[35] J. Li, Z. Wang, *J. Power Sources* **2020**, *450*, 227648.
[36] Y. Wang, H. Ming, J. Qiu, Z. Yu, M. Li, S. Zhang, Y. Yang, *J. Electroanal. Chem.* **2017**, *802*, 8–14.
[37] N. Ehteshami, L. Ibing, L. Stolz, M. Winter, E. Paillard, *J. Power Sources* **2020**, *451*, 227804.
[38] V. Aravindan, Y. L. Cheah, W. C. Ling, S. Madhavi, *J. Electrochem. Soc.* **2016**, *159*, 1435–1439.
[39] N. V. Kosova, O. A. Podgornova, E. T. Devyatkina, V. R. Podugolnikov, S. A. Petrov, *J. Mater. Chem. A* **2014**, *2*, 20697–20705.
[40] K. Subramanyan, Y. S. Lee, V. Aravindan, *J. Colloid Interface Sci.* **2021**, *582*, 51–59.
[41] E. Markevich, R. Sharabi, H. Gottlieb, V. Borgel, K. Fridman, G. Salitra, D. Aurbach, G. Semrau, M. A. Schmidt, N. Schall, C. Bruenig, *Electrochem. Commun.* **2012**, *15*, 22–25.
[42] R. Sharabi, E. Markevich, V. Borgel, G. Salitra, G. Gershinsky, D. Aurbach, G. Semrau, M. A. Schmidt, N. Schall, C. Stinner, *J. Power Sources* **2012**, *203*, 109–114.
[43] J. Cha, J. G. Han, J. Hwang, J. Cho, N. S. Choi, *J. Power Sources* **2017**, *357*, 97–106.
[44] T. Q. Nguyen, C. Breitkopf, *J. Electrochem. Soc.* **2018**, *165*, E826–E831.
[45] X. Wu, M. Meledina, H. Tempel, H. Kungl, J. Mayer, R. Eichel, *J. Power Sources* **2020**, *450*, 227726.

Manuscript received: August 1, 2022
Revised manuscript received: September 16, 2022
Accepted manuscript online: September 16, 2022